

# A decade of horizontal deformation from great earthquakes

P. Tregoning<sup>1</sup>, R. Burgette<sup>2,3</sup>, S.C. McClusky<sup>1</sup>, S. Lejeune<sup>4</sup>, C.S. Watson<sup>2</sup>, H. McQueen<sup>1</sup>

**Abstract.** The 21st Century has seen the occurrence of 17 great earthquakes ( $M_w > 8$ ), including some of the largest earthquakes ever recorded. Numerical modelling of the earthquakes shows that nearly half of the Earth's surface has undergone horizontal co-seismic deformation  $> 1$  mm, with the 2004 Sumatra-Andaman earthquake dominating the global deformation field. This has important implications for both the realisation of a terrestrial reference frame and in the interpretation of regional tectonic studies based on GPS velocities. We show that far-field co-seismic deformations from great earthquakes will, if unaccounted for, introduce errors in estimates of linear site velocities of at least 0.1–0.3 mm/yr across most of the surface of the Earth. The accumulated global deformation field shows that two regions, Australia and the north Atlantic/Arctic Ocean, have been largely undeformed by these great earthquakes, with accumulated deformations generally  $< 0.5$  mm. Using GPS estimates of surface deformation, we show that the majority of the Australian continent is deforming at  $< 0.2$  mm/yr, the northern part of New Zealand is rotating clockwise relative to the Australian Plate with relative horizontal velocities of  $\sim 2$  mm/yr, while the southeastern coast of Australia is undergoing post-seismic relaxation caused by the 2004  $M_w = 8.1$  Macquarie Ridge earthquake. The presence of ongoing post-seismic relaxation thousands of kilometres from plate margins violates the secular/linear assumption made in current terrestrial reference frame definitions. These effects have significant ramifications for regional tectonic interpretations and global studies such as sea level rise that require reference frame accuracy greater than this level.

## 1. Introduction

Strain accumulation and release within the Earth's tectonic plates occurs over a wide range of spatial and temporal scales throughout the seismic cycle. Conventional plate tectonic theory is built around the premise that the plates are rigid, an assumption that underpins the coordinate reference frames relied upon by Earth-observing space missions for measuring the dynamic Earth system [e.g. *Altamimi et al.*, 2012]. Today's modern space geodetic techniques enable the determination with unprecedented precision of where, when and at what rate tectonic plates are deforming.

Whether tectonic plates behave as rigid bodies has ramifications for how the surface of the Earth evolves over time. The coordinate reference frame used on Earth underpins many scientific studies (e.g. sea level rise, crustal deformation, satellite orbit estimation etc) and its accuracy relies upon representing correctly the temporal movement of the tracking stations on Earth. The assumption that tectonic plates move as rigid bodies implies that site velocities will be linear on short time scales, and to what extent this assumption is correct directly affects our ability to construct accurately a temporally varying reference frame. It is timely to re-address the question of the rigidity of tectonic plates

in light of the occurrence of great megathrust earthquakes that have deformed the Earth over many thousands of kilometres [e.g. *Kreemer et al.*, 2006]. What upper bound can be placed on the rigidity of large tectonic elements, particularly those regions that are distant from great earthquakes, and how do assumptions of large-scale plate rigidity affect regional tectonic studies?

Detection of far-field co-seismic displacements greater than a few millimetres caused by the Sumatra-Andaman earthquake [e.g. *Vigny et al.*, 2005; *Fu and Sun*, 2006; *Kreemer et al.*, 2006] show the power of using Global Positioning System (GPS) estimates to quantify global deformation, although very distant (i.e.  $> 1000$  km) displacements caused by the smaller of the great earthquakes have not previously been identified. Recent improvements in the analysis of GPS observations [e.g. *Boehm et al.*, 2006] have provided the ability to detect temporal variations in site movements at the sub-mm level [e.g. *Steigenberger et al.*, 2009; *Tregoning and Watson*, 2009, 2011], and to make velocity estimates with a precision of 0.3 mm/yr [*Altamimi et al.*, 2012]. This improvement offers the potential to identify regions where the crust is more stable than these detection levels and, importantly, the ability to detect very far-field co-seismic displacements and post-seismic deformation.

In this study we calculate the global pattern of co-seismic deformation from 15 earthquakes  $M_w > 8$  since 2000 using a spherical elastic dislocation model. Modelled far-field deformations are of comparable size and typically small (i.e.  $< 1-2$  mm) in both horizontal and vertical components. For the vertical deformations, this level of deformation is well below the inherent noise levels in current GPS analyses, caused by noise introduced through the mismodelling of tropospheric effects [e.g. *Steigenberger et al.*, 2009; *Tregoning and Watson*, 2009], ocean tide and non-tidal ocean loading effects [e.g. *Williams and Penna*, 2011] and spurious periodic signals that have aliased through the estimation process to harmonics of the GPS draconitic year (351.4 days) [e.g. *Ray et al.*, 2008; *Tregoning and Watson*, 2009]. As a result, not

<sup>1</sup>Research School of Earth Sciences, The Australian National University, Canberra, ACT, Australia

<sup>2</sup>Surveying and Spatial Science Group, School of Geography and Environmental Studies, University of Tasmania, Hobart, TAS, Australia

<sup>3</sup>Now at Department of Geological Sciences, University of Oregon, Eugene, Oregon, USA

<sup>4</sup>Royal Meteorological Institute of Belgium, Brussels, Belgium

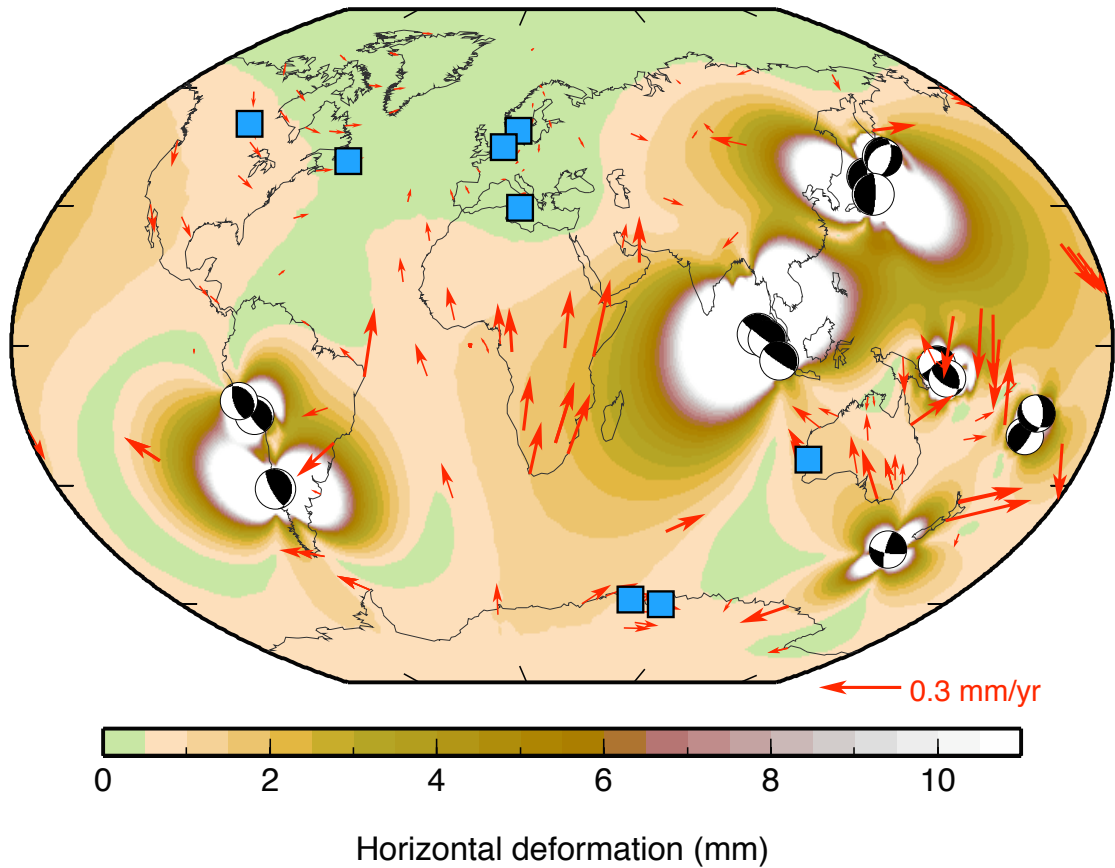


**Figure 1.** Accumulated co-seismic horizontal deformation field of great earthquakes ( $M_w > 8$ ) since 2000. Focal mechanisms are from the Global Moment Tensor catalog [Ekström et al., 2012]. GPS sites used to define the terrestrial reference frame are shown (blue squares), along with far-field site velocity errors (red arrows) induced by not accounting for the co-seismic horizontal deformations of the great earthquakes

accounting for vertical co-seismic deformations at far-field sites will have an undetectable effect on the reference frame used in GPS analysis at the present time. We therefore limit our analysis to the horizontal components where the deformation is detectable, and hence must be considered.

In this study we calculate the global pattern of co-seismic deformation from 15 earthquakes  $M_w > 8$  since 2000 using a spherical elastic dislocation model. We use the Australian Plate as a case study to demonstrate how the realisation of the coordinate reference frame in the GPS analysis can lead to different tectonic interpretations, and show that significant crustal deformation effects occurring thousands of kilometres from plate boundary zones might be overlooked unless far-field horizontal deformation from great earthquakes are taken into consideration. Focusing on the Australasian region, we compare our modelled co-seismic horizontal deformations with those estimated from time series of positions derived from a decade of global GPS data. Finally, after accounting for non-tectonic (instrumental) offsets in the time series, we assess the level of rigidity and physical extent of the rigid Australian Plate.

## 2. Earthquake Modelling

We derived model estimates of static co-seismic deformation using a spherical layered model [Pollitz, 1996]. Surface deformation is calculated assuming the PREM elastic stratification [Dziewonski and Anderson, 1981], with a spherical harmonic expansion from degrees 1 to 1500. Below we describe the modelling of 15 earthquakes of  $M_w > 8$  (Table 1) that have occurred since 2000 [Ekström et al., 2012]. These

calculations assume a static Earth, and our investigation focuses on the horizontal distortion of the Earth's surface by great earthquakes. We use a variety of rupture and slip distribution models, prioritising published results that explicitly specify the spatial extent of slip on fault planes. For events that lack published slip distribution information in tabular form, we generalised fault planes with uniform slip over an area approximately coincident with that estimated from published teleseismic investigations, and a magnitude of slip consistent with the moment magnitude estimated in the seismic investigation(s) (for far-field deformation, the actual details of the slip distribution are much less important than for modelling near-field deformation and we found  $< 0.5$  mm differences in modelled far-field co-seismic deformations when using different rupture and slip distribution models). Fault parameters for which we have assumed a uniform slip model are provided in the supplementary material (Table S1).

### 2.1. Great Earthquakes

#### 2.1.1. 2000 Papua New Guinea

We model the 16 November 2000 Mw 8.0 New Ireland area earthquake as left-oblique reverse slip on the Weitin Fault, with the geometry and rake of the rupture from a seismic study [Park and Mori, 2007]. We constrain the moment to the value from the Global Centroid Moment Tensor project (GCMT) [Ekström et al., 2012], which is intermediate among the reported estimates [Park and Mori, 2007].

#### 2.1.2. 2001 Peru

We model the 23 June 2001 Mw 8.5 Arequipa, Peru earthquake with uniform slip on a single plane coincident with the area of the majority of the slip as inferred by a joint seismic and geodetic study [Pritchard *et al.*, 2007]. The rake and moment are mean values [Pritchard *et al.*, 2007].

#### 2.1.3. 2003 Japan

The 25 September 2003 Mw 8.1 Tokachi-Oki earthquake occurred along the southwestern Kuril Trench. We model the earthquake using a slip distribution constrained by GPS and tsunami observations [Romano *et al.*, 2010].

#### 2.1.4. 2004 Macquarie Ridge

The 23 December 2004 Mw 8.2 earthquake occurred as strike-slip on a fracture zone west of Macquarie Ridge in the Australian plate. We use a previously published fault geometry derived from seismic locations and regional GPS observations [Watson *et al.*, 2010], with an updated inversion for slip using Greens functions calculated with the spherical layered elastic model [Pollitz, 1996]. The mean horizontal velocity residual is reduced to 1.2 mm, and the estimated moment is approximately double that inferred from a non-spherical homogeneous elastic half-space [Watson *et al.*, 2010].

#### 2.1.5. 2004 Sumatra-Andaman

The 26 December 2004 Mw 9.2 earthquake ruptured the northern Sumatra and Andaman portions of the Indo-Australian-Eurasia plate boundary. We use a static slip distribution [Banerjee *et al.*, 2007] (model C) derived from the spherical layered deformation code [Pollitz, 1996] used here and regional GPS displacements.

#### 2.1.6. 2005 Sumatra

The 28 March 2005 Mw 8.7 Nias earthquake ruptured the northern Sumatra megathrust immediately south of the 2004 great earthquake. We again use the slip distribution from a geodetic study [Banerjee *et al.*, 2007].

#### 2.1.7. 2006 Tonga

The 5 May 2006 Mw 8.0 earthquake occurred along the Tonga subduction zone. We model the earthquake using a single plane with uniform slip. The geometry and extent are constrained by plate boundary orientation, GCMT [Ekström *et al.*, 2012] parameters and aftershocks. We use GCMT estimates to constrain the moment and slip direction. Our source model is similar to that used in a tsunami study [Tang *et al.*, 2008].

#### 2.1.8. 2006 Kuril Islands

The 15 November 2006 Mw 8.3 thrust earthquake ruptured a portion of the Kuril subduction fault. We model this earthquake with a uniform slip, planar fault approximately coincident with the area of  $> 1$  m slip reported in a seismic investigation [Lay *et al.*, 2009]. The mean slip orientation is taken from this seismic study, and we constrain the slip magnitude such that the moment is equal to the GCMT solution [Ekström *et al.*, 2012]. The GCMT magnitude is intermediate amongst several estimates [Lay *et al.*, 2009].

#### 2.1.9. 2007 Kuril Islands

The 13 January 2007 Mw 8.1 earthquake occurred as normal faulting in the subducting Pacific Plate, immediately east of the 2006 rupture. As with the 2006 event, we model the deformation using a geometry and slip direction based on a finite fault seismic inversion [Lay *et al.*, 2009], and an intermediate estimate of moment from the GCMT [Ekström *et al.*, 2012].

#### 2.1.10. 2007 Solomon Islands

The 1 April 2007 Mw 8.1 Solomon Islands earthquake occurred as dominantly thrust slip along the Solomon Islands subduction zone across a triple junction. We model the earthquake assuming uniform slip with moment and average slip direction as inferred from seismic observations [Furlong

*et al.*, 2009]. The extent of the rupture plane is constrained by aftershocks and the spatial extent of the slip from the seismic finite fault inversion.

#### 2.1.11. 2007 Peru

The 15 August 2007 Mw 8.0 Pisco, Peru earthquake ruptured a section of the South America-Nazca plate boundary north of the axis of the subducting Nazca ridge. We use a slip distribution jointly constrained with seismic and InSAR observations [Sladen *et al.*, 2010]. (downloaded from [http://www.tectonics.caltech.edu/slip\\_history/2007\\_peru/pisco-update.html](http://www.tectonics.caltech.edu/slip_history/2007_peru/pisco-update.html))

#### 2.1.12. 2007 Sumatra

The 12 September 2007 Mw 8.4 southern Sumatra earthquake ruptured a portion of the Sumatra megathrust farther to the southeast than the 2005 earthquake. We use a slip distribution constrained with seismic and geodetic observations [Konca *et al.*, 2008]. (downloaded from [http://www.tectonics.caltech.edu/slip\\_history/2007\\_s.sumatra/ssuma-update.html](http://www.tectonics.caltech.edu/slip_history/2007_s.sumatra/ssuma-update.html))

#### 2.1.13. 2009 Samoa-Tonga

The 29 September 2009 great earthquake doublet involved contemporaneous or nearly contemporaneous slip on both the Tonga subduction thrust interface and a normal fault in the subducting Pacific Plate, with each sub-event having a moment magnitude of 8.0 [Lay *et al.*, 2010; Beavan *et al.*, 2010]. Here, we use the two fault source model inferred from GPS and tsunami observations [Beavan *et al.*, 2010].

#### 2.1.14. 2010 Chile

The 27 February 2010 Mw 8.8 megathrust earthquake ruptured the South America-Nazca plate boundary in the Maule, Chile region. We use a slip distribution constrained by geodetic and tsunami data [Lorito *et al.*, 2011].

#### 2.1.15. 2011 Japan

The 11 March 2011 Mw 9.0 Tohoku-Oki thrust earthquake ruptured a portion of the Pacific-Okhotsk plate boundary. We use a static slip distribution constrained by GPS and tsunami observations [Simons *et al.*, 2011]. In our model, the complex triangular sub-fault geometry is approximated with 227 rectangular subfaults that include one along-strike change in the strike direction, and a change in dip with depth that is averaged along-strike. We resample the published slip distribution to our geometry such that the spatial distribution of slip magnitude and azimuth are preserved.

## 2.2. Accumulated deformation

The accumulated modelled co-seismic horizontal deformation caused by these events exceeds 1 mm over much of the Earth (Figure 1) and is dominated by the contribution of the Sumatra-Andaman earthquake, with lobes of deformation spreading NE and SW from the megathrust boundary. We calculate co-seismic horizontal displacements as far afield as Flin Flon in central Canada (0.7 mm), 1.5 mm at Capetown, South Africa and 0.5 mm in Santiago, Chile. This is in general agreement with the computations of, for example *Fu and Sun* [2006] but is notably smaller in magnitude across Africa and South America than the results of *Kreemer et al.* [2006] (the spherical layer model code of *Pollitz* [1996] did not accurately calculate deformation over the longest spatial scales. The version of code used in this study is appropriate for full global calculations (F. Pollitz, *pers. comm.*, July 2011)). Modelling shows that the regions in the direction of the prolongation of the strike of the thrust (i.e. NW across Europe and SE across Australia) experienced much smaller co-seismic horizontal deformations, with magnitudes  $< 0.5$  mm (Figure 2a).

In contrast, the February 2011 Tohoku-Oki earthquake caused smaller far-field co-seismic horizontal deformations because a significant part of the energy release occurred at

**Table 1.** Great earthquakes whose co-seismic horizontal deformation is modelled in this study.

#	Earthquake	Date	Magnitude	Source
1	New Ireland, PNG	2000-11-16	8.0	<i>Park and Mori</i> , [2007]
2	South Peru	2001-06-23	8.4	<i>Pritchard et al.</i> , [2007]
3	Hokkaido, Japan	2003-09-25	8.3	<i>Romano et al.</i> , [2010]
4	Macquarie Island	2004-12-23	8.1	<i>Watson et al.</i> , [2010]
5	Sumatra-Andaman	2004-12-26	9.3	<i>Banerjee et al.</i> , [2007]
6	Northern Sumatra	2005-03-28	8.6	<i>Banerjee et al.</i> , [2007]
7	Tonga	2006-05-03	8.0	<i>Ekström et al.</i> , [2012]
8	Kuril Islands	2006-11-25	8.3	<i>Lay et al.</i> , [2009]; <i>Ekström et al.</i> , [2012]
9	East of Kuril Islands	2007-01-13	8.1	<i>Lay et al.</i> , [2009]; <i>Ekström et al.</i> , [2012]
10	Solomon Islands	2007-04-01	8.1	<i>Furlong et al.</i> , [2009]
11	Central Peru	2007-08-15	8.0	<i>Sladen et al.</i> , [2010]
12	Southern Sumatra	2007-09-12	8.5	<i>Konca et al.</i> , [2008]
13	Samoa	2009-09-29	8.1	<i>Lay et al.</i> , [2010]; <i>Beavan et al.</i> , [2010]
14	Maule, Chile	2010-02-27	8.8	<i>Lorito et al.</i> , [2011]
15	Tohoku-Oki, Japan	2011-03-11	9.1	<i>Simons et al.</i> , [2011]

depths greater than 30 km [e.g. *Yagi and Fukahata*, 2011], thus reducing the magnitude of the induced surface deformations. The energy release was also smaller than the Sumatra-Andaman earthquake [*Ekström et al.*, 2012]. The lobes of major deformation extend to the east (into the Pacific) and west of Japan, affecting eastern Europe but again essentially missing the Australian region (Figure 2b). The other earthquakes with magnitudes  $8 < M_w < 9$  caused co-seismic horizontal displacements of several metres in the near-field regions but, at distances  $> 1000$ - $2000$  km, the displacement field reduces to  $< 1$  mm. Thus, viewed from a global perspective, these earthquakes have a more minor effect on the total deformation of the Earth (Figure 2c). The Australian continent, western Europe and the eastern tip of Canada are the only subaerial regions with an average co-seismic horizontal deformation less than 0.5 mm (Figure 1).

We find that the magnitude of slip required to explain the observed deformation pattern of the 2004 Macquarie Ridge earthquake is 80% greater than previously reported [*Watson et al.*, 2010]; however, the model in that study was a flat-Earth, layered model whereas we use here a spherical, homogeneous half-space elastic dislocation model. Our new model predicts deformation of up to 1 mm further north and northwest into the Australian continent (see Figure 2c); however, we do not detect these deformations in our GPS time series. This discrepancy is similar to tests presented by *Banerjee et al.* [2007], who attributed the differences to the consequences of layered elastic properties and sphericity assumptions, where the latter reduces the discrepancy with greater distance.

### 3. Data Analysis

#### 3.1. GPS analysis and reference frame definition

Our GPS analysis of over 100 global sites was performed with the GAMIT software [*Herring et al.*, 2010], employing time-varying modelling of atmospheric delays, mapping functions and atmospheric pressure loading deformation [*Tregoning and Watson*, 2009, 2011]. We aligned our daily, global GPS solutions from 2000 to 2011.0 with the International Terrestrial Reference Frame 2008 [*Altamimi et al.*, 2011] by computing 6-parameter transformations (3-rotations, 3-translations) of the coordinates of the 8 reference sites listed above (Figure 1 and described below). A significant co-seismic displacement ( $\sim 0.7$  mm) at the time of the Sumatra-Andaman earthquake was detected and removed at site Flin Flon (FLIN); otherwise, no significant earthquake deformations were apparent at these reference sites.

#### 3.2. Reference frame definition

A fundamental reference frame is defined by an origin, three orthogonal axes and scale [*Altamimi et al.*, 2011]. For the International Terrestrial Reference Frame (ITRF), the

origin is defined from the analysis of Satellite Laser Ranging (SLR) measurements to satellites orbiting the centre of mass of the Earth such that there are zero translations and rotation rates with respect to the centre of mass of the Earth, while the scale is defined from the mean of scale estimates from SLR and Very Long Baseline Interferometry (VLBI) long-term solutions [*Altamimi et al.*, 2011]. The realisation of the terrestrial reference frame - and the way that users of the frame can access the information - is through the use of the coordinates of sites located on the surface of the Earth.

The fact that much of the Earth is affected by co-seismic deformation from these great earthquakes is problematic for the definition of the terrestrial reference frame that is used to underpin all geophysical studies using space geodetic techniques. Because the co-seismic displacement field caused by each earthquake occurs over a matter of seconds to minutes (GPS solutions are typically averaged to daily or weekly values) it becomes difficult to estimate the offsets at individual sites, particularly when many sites may have been displaced simultaneously. What then is the effect of unmodelled co-seismic displacements on the definition of the reference frame? Earthquakes have a strong tendency to deform the shape of the Earth towards being less oblate [*Chao and Gross*, 1987]; one should question to what extent the centre of mass of the Earth changes as a result of any earthquake, but great earthquakes in particular since the deformation pattern can cover much of the Earth.

If the centre of mass of the Earth were to move with respect to the surface of the Earth because of co-seismic deformation then the entire set of coordinates required to define the ITRF would have to change because the pre- and post-earthquake vectors between a site on the surface and the origin would be different. Even the coordinates of a site located in a region that did not undergo far-field deformation would be different before and after an earthquake if the origin of the coordinate system changed location.

*Gross and Chao* [2006] assessed the effect of the 2004 Sumatra-Andaman earthquake on the rotation and the gravity field of the Earth. They computed that the length-of-day would have decreased by 6.8 milliseconds, the pole of rotation would have moved by 2.32 milliarcseconds and that the Earth's oblateness would have reduced by  $2.37 \times 10^{-11}$ . They concluded that the rotational effects were smaller (by a factor of  $\sim 3$ ) than the current observational accuracy but that the change in oblateness should be detectable. Importantly, their study made the assumption that the origin of the coordinate system was at the centre of mass of the Earth (i.e. that the degree-1 terms of the change in gravitational potential were zero); that is, that the origin didn't move as a result of the earthquake. Thus, no consideration was given to the problem articulated above concerning earthquake induced movement of the centre of mass of the Earth relative to the surface.

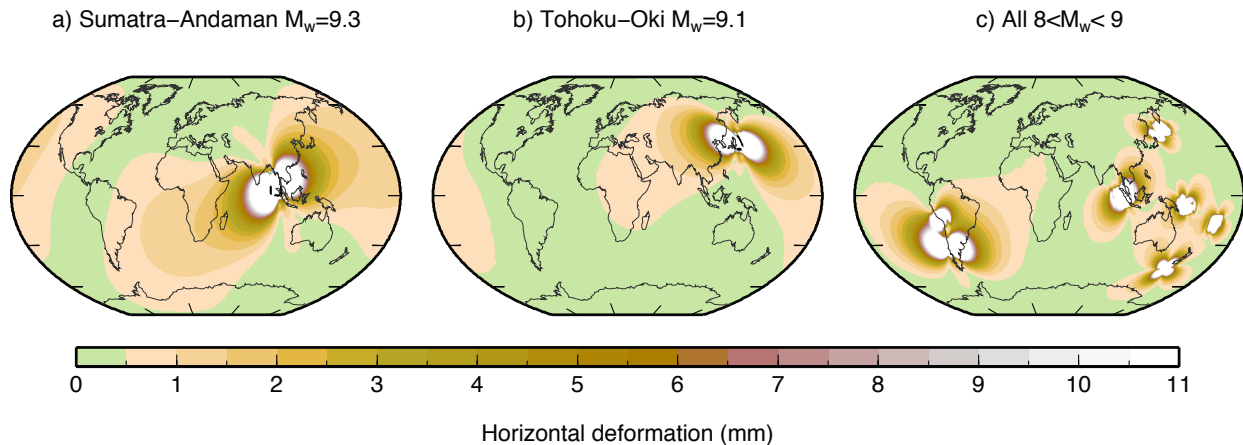


**Figure 2.** Magnitude of co-seismic horizontal deformation of the a) Sumatra-Andaman, b) Tohoku-Oki earthquakes and c) the sum of all other great earthquakes since 2000.

Because it is predominantly the surface shell that deforms in a shallow megathrust event, we computed the change in centre of mass of a 10 m thick shell at the surface of the Earth (assuming a spherical Earth) for the modelled co-seismic deformations of the Sumatra-Andaman earthquake, the largest recorded great earthquake. The translation of the origin induced by the deformation was 0.3 mm, 0.9 mm and -1.3 mm for the X, Y and Z components, respectively (we used a mean density of  $3000 \text{ kg/m}^3$  in our computations). However, when the interior of the Earth is added to the computation these values decrease to  $< 3$  nanometres. Thus, we find that there is no significant change in the location of the centre of mass of the Earth as a result of great earthquakes, and we do not consider any further this effect. However, there still remains the problem of the co-seismic deformations changing the ITRF coordinates of sites on the surface of the Earth.

We address this problem by using a ‘stable site’ approach of carefully selecting sites in regions with modelled displacements of  $< 1$  mm (see Figure 1) to define our reference frame. We assume that the coordinates of these sites are the same after the earthquake as before it. This then imposes the assumption that the origin has not moved. We then use this realisation of the reference frame (which is essentially the ‘pre-earthquake’ reference frame) to calculate changes in coordinates of sites in deformed areas. We selected three sites in Europe (Westerbroek, The Netherlands; Onsala, Sweden; Noto, Italy), two sites in North America (St Johns, Canada; Flin Flon, Canada), two sites in Antarctica (Mawson and Davis) and one site in Australia (Yarragadee). Each of these sites has operated with minimal interruptions from 2000.0 to 2011.0, has a low amplitude of hydrological surface deformation [Tregoning *et al.*, 2009] and is present in over 95% of our daily GPS solutions.

Our tests showed that the use of merely 8 sites is sufficient to define a stable reference frame over the 2000-2011 period; indeed, including only one site per continent is sufficient to generate stable coordinate time series. We identified offsets in the time series of these 8 sites (caused by equipment changes plus the co-seismic deformation at Flin Flon during the the Sumatra-Andaman earthquake) through constraining only four sites and then assessing the time series of the other four sites, then reversing the selection of reference sites. Once all offsets were removed from the time series of our reference sites, we were able to use all 8 sites without fear of introducing biases into the coordinate estimates of the global network as a result of discontinuities in our reference frame definition.

This approach generates time series of coordinate estimates that are less affected by the non-stationary variations of surface deformation at reference sites when substantially

more reference sites are used. Of course, a bootstrapping process could be used to identify and correct for co-seismic displacements at other sites; however, this may introduce additional noise (caused by hydrological loading) and, for the purposes of this study, the use of only these 8 sites provides a stable reference frame definition.

### 3.3. Offsets in time series

The presence of Heavyside steps or offsets in time series is problematic when trying to estimate linear trends from observations. Our coordinate time series have a sufficiently low level of noise that we can estimate directly statistically significant offsets (sometimes as small as 0.5 mm) induced by instrument-related effects such as changes in antenna/receiver hardware and receiver firmware upgrades. Earthquake-related offsets can only be derived from individual time series because the deformation signals cancel out in differenced time series if the baselines are short, whereas instrument-related offsets can be derived either from individual coordinate time series or by differencing time series with nearby sites. We relied on the IGS site logs to provide accurate dates of changes in site hardware in addition to ITRF2008 discontinuities, and estimated offsets at these times. We used the ‘real sigma’ approach described in Reilinger *et al.*, [2006] to model realistically the noise of the GPS time series, then selected only estimated offsets that were different from zero at the  $3\sigma$  level.

For example, in Canberra, three IGS sites operate within 30 km: one at Tidbinbilla (TIDB) and two at Mt Stromlo (STR1, STR2). We identified a total of four instrument-related horizontal offsets at these sites - all  $< 2.3$  mm - through an assessment of differenced position time series. This approach yielded independent estimates that were found to be compatible at  $< 0.2$  mm. Importantly, the estimates derived from each individual time series alone differ by more than this level and we consider the ‘absolute’ estimates to be less accurate, given the influence of time-correlated noise.

We subsequently used the differenced time series approach to assess potential offsets at all sites on the Australian Plate and identified significant offsets at Yarragadee (YAR2), Ceduna (CEDU), Darwin (DARW) and Auckland (AUCK). This is the same approach that we used at each of our reference sites, generating differenced time series to nearby sites in order to estimate the equipment-induced offsets at the reference sites.

The use of differenced time series from multiple sites co-located within several hundred metres provides a very accurate means of identifying sub-mm offsets introduced through

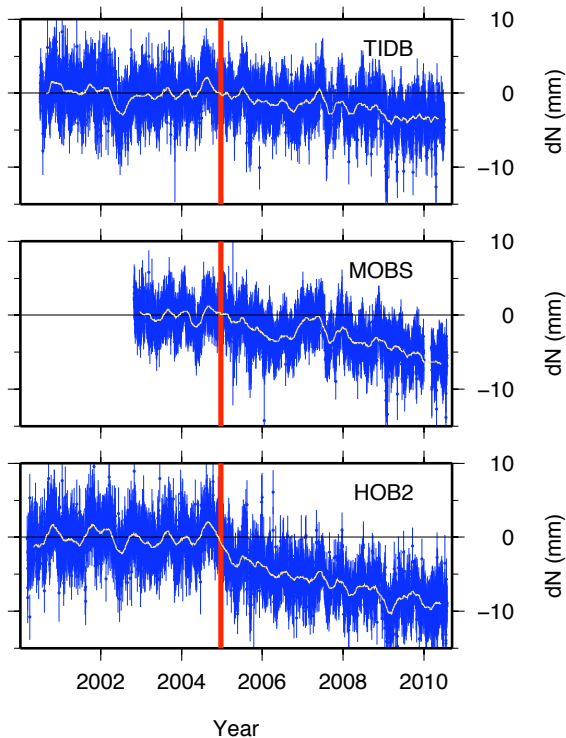


**Figure 3.** GPS time series of the north components at Hobart (HOB2), Melbourne (MOBS) and Canberra (TIDB), detrended over the pre-earthquake period (2000-2004.9). 100-day running mean is plotted. Vertical lines indicate the date of the Macquarie Island earthquake. Site locations are indicated on Figure 5.

instrument changes at any of the co-located sites (so long as firmware upgrades are not performed simultaneously at all sites). This provides strong support for the recommendations of the Global Geodetic Observing System that all key infrastructure sites in the global GPS network should have multiple sets of equipment observing simultaneously [Rothacher *et al.*, 2009].

### 3.4. Induced velocity errors

What is the effect of small, uncorrected co-seismic deformations on estimates of linear site velocities? We assessed this over the period of our analysis (2000.0 to 2011.0) by generating time series of modelled co-seismic displacements at each GPS site in our global network as caused by the 15 great earthquakes. The trend of each time series then provides an estimate of the likely error that will be induced in velocity estimates if the far-field co-seismic horizontal displacements are not accounted for (note that we are not considering here the inter-seismic strain accumulation that may occur at far-field sites; rather, simply the error in the linear trend estimates that the presence of co-seismic discontinuities cause. The inter-seismic strain issue is likely to be a second-order effect and is not discussed in this study).

We found that the horizontal velocity errors reach 0.2-0.4 mm/yr (Figure 1), even though the accumulated displacement from the great earthquakes amounts to only a few millimetres (of course, the magnitude of the error is a function of the time of the earthquake with respect to the time span of the GPS time series; however, we have generated these estimates using the actual timing of the great earthquakes over the past decade and so the errors are realistic). This level of error would degrade the accuracy of the terrestrial reference frame, potentially affecting the ability to estimate

satellite orbits with sufficient accuracy to enable estimates of geophysical processes (e.g. sea level rise) with mm accuracy [Beckley *et al.*, 2007]. We show in Section 4 that the errors can also affect continent-scale tectonic interpretations.

Co-seismic deformations exceeding  $\sim 5$  mm are often reported in the near- to medium-field [e.g. Kreemer *et al.*, 2006] and are accounted for in geophysical studies (i.e. sites located in the white regions of Figure 1); however, velocity errors will occur further afield as a result of the smaller, more distant co-seismic deformations. Of particular note is the spatial coherence of the velocity errors in some regions which would propagate into models of rigid plate rotations derived from GPS velocities estimated at the sites. Indeed, the velocity errors of 9 sites in southern and central Africa (see Figure 1) can be modelled by a single pole of rotation with an accuracy of  $\sim 0.02$  mm/yr and induce a rotation error of  $\sim 0.02^\circ$ /My into the definition of the Euler vector for the African Plate (around 7% of the actual plate rotation rate). Thus, far-field co-seismic deformations will affect independent tectonic studies thousands of kilometres away from the earthquake rupture zones unless properly accounted for.

## 4. Case Study: Intra-plate deformation of the Australian Plate

In this section we undertake a typical tectonic study of the stability of a continental plate. We use this to demonstrate to what extent local tectonic studies can be affected by the horizontal deformations induced by far-field earthquakes and also to show how the selection of the strategy used to realise the coordinate reference frame can affect the tectonic interpretation.

The amount of deformation of the Australian Plate from great earthquakes has been low this century when compared to other regions of the Earth. Australia is also one of the largest continental portions of a tectonic plate that does not have a diffuse plate boundary zone [Gordon, 1998] and is not experiencing rapid rates of horizontal motion due to present-day glacial isostatic adjustment (as is the case in, for example North America and Europe). We therefore used GPS velocity estimates on this continent to assess to what extent a plate appears to be ‘rigid’ over the first decade of the 21st Century. Nonetheless, before intra-plate stability can be examined, we must first correct for small co-seismic horizontal deformations that have occurred within the Australian Plate as a result of the distant great earthquakes: the 2007 Solomon Islands earthquake caused a significant ( $\sim 1.7$  mm) co-seismic displacement at Townsville in north-east Australia, the 2004 Sumatra-Andaman earthquake displaced the GPS site at Darwin by 1.7 mm while the Macquarie Ridge earthquake displaced Hobart (HOB2) by  $\sim 5$  mm [Watson *et al.*, 2010]. No earthquake deformations were found to be statistically significantly different from zero at any other sites on mainland Australia.

The modelled far-field deformations typically lie within the error ellipses of the GPS estimates of co-seismic deformation (at the 95% confidence level). (Figure 4). This provides confidence in the far-field deformation modelling of the co-seismic horizontal deformation field and also that the GPS offset estimates are detecting geophysical signal at the times of the earthquakes rather than just noise. While we did not rely on the earthquake models to correct our GPS time series for co-seismic displacements (we estimated offsets directly from the time series themselves), this qualitative comparison demonstrates that the use of far-field GPS data is sensitive to these large-scale geophysical processes.

We identify a small but consistent non-linear, post-seismic relaxation deformation in the GPS time series of

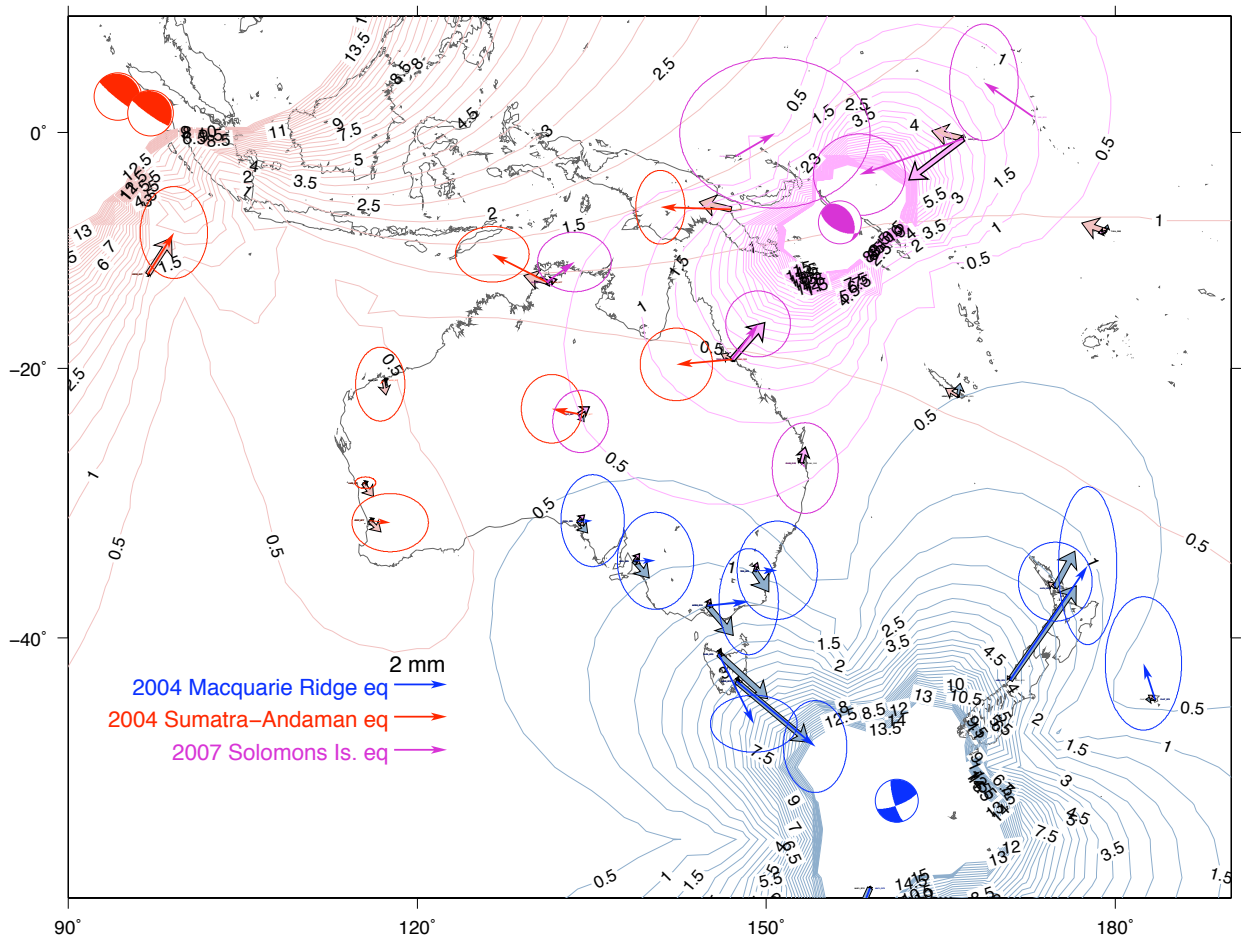


**Figure 4.** Co-seismic horizontal displacements at GPS sites located on the Australian Plate. Focal mechanisms of the Sumatra-Andaman (red), Macquarie Island (blue) and Solomon Islands (pink) earthquakes were sourced from the Global Central Moment Catalogue. Contours of the magnitude of co-seismic horizontal deformation for each earthquake are plotted along with the predicted horizontal displacements (thicker arrows, colour-coded for each earthquake).

sites along the eastern coast of Australia, decreasing with distance northward from the Macquarie Ridge earthquake epicentre. This is most prominent in the north component (Figure 3) and is actually of significantly greater magnitude than the co-seismic deformation. Neither the co-seismic deformation nor variations in the site velocity at Hobart, Melbourne or Canberra were identified in the most recent determination of the International Terrestrial Reference Frame [Altamimi *et al.*, 2011]; therefore, the ITRF2008 does not account for this far-field earthquake deformation in southeastern Australia. This may explain some of the larger (i.e.  $> 0.4$  mm/yr) residual velocities found by Altamimi *et al.* [2012] for sites on the Australian Plate. Because of the presence of ongoing post-seismic deformations at Hobart, Melbourne and Canberra (Figure 3), the velocities of these sites after the earthquake should no longer be represented by linear models.

Once corrected for instrument offsets (see Section 3.3), site velocities were estimated from the time series, with associated uncertainties derived using the ‘real sigma’ approach [Reilinger *et al.*, 2006] to account for the non-gaussian nature of GPS time series. Typical levels of uncertainties were  $\sim 0.3$  mm/yr for sites with  $> 10$  year data spans and  $\sim 1$  mm/yr for sites with 2-5 year data spans. For the sites in southeastern Australia undergoing post-seismic deformation, we estimated a linear site velocity for only the time period before the 2004 Macquarie Ridge earthquake.

Previous GPS studies have identified the Australian Plate as being a region of recent crustal stability, with internal de-

formation rates of  $< 2$  mm/yr [Tregoning, 2003; Sella *et al.*, 2007; Altamimi *et al.*, 2012]. We inverted our site velocities to estimate an Euler vector to represent the rigid plate rotation of the Australian Plate. Several sites show significant horizontal motion with respect to the rigid plate motion: Perth (PERT) and Hillarys (HIL1) in southwestern WA and the southeastern GPS sites at HOB2, MOBS and TIDB. We attribute the motion of the first two sites to the extraction of groundwater [Featherstone *et al.*, 2012]. Indeed, the vertical velocities of these sites (not shown) identify subsidence of  $\sim 3$  mm/yr over the past decade. The residual velocities of sites along the east coast of Australia may reflect inter-seismic strain accumulation prior to the 2004 Macquarie Ridge and 2007 Solomon Island earthquakes. We note that Altamimi *et al.* [2012] did not include HIL1, PERT or MOBS in the estimation of the rigid motion of the Australian Plate.

After removing these 5 sites from the inversion, the remaining 6 sites show relative velocity vectors of  $< 0.2$  mm/yr with respect to a rigid plate motion model for the Australian Plate (Figure 5). Our residual velocities at these sites have a root-mean-square (RMS) of 0.15 mm/yr and 0.16 mm/yr for north and east, respectively - smaller than those of Altamimi *et al.* [2012] with a RMS of 0.17 mm/yr and 0.21 mm/yr for north and east, respectively for the velocity residuals of the same sites. This represents a reduction in RMS of around 11% and 23%.

We interpret our value of 0.2 mm/yr to indicate an upper bound on the magnitude of current intraplate deformation

across the Australian continent. However, it is clear that co- and post-seismic deformation is considerable even thousands of kilometres from the epicentres of the great earthquakes that have occurred around the fringe of the Australian Plate. The fact that co-seismic deformation occurs implies that inter-seismic strain accumulation would have occurred prior to the earthquake ruptures, perhaps over decades to hundreds of years. Therefore, large tectonic plates should not be modelled as rigid bodies, and models of tectonic motion implicit in the definition of the terrestrial reference frame need to be more complex than simply representing continental drift with a linear velocity.

#### 4.1. New Zealand

We now apply our plate model and GPS analysis to address the question of whether the North Island of New Zealand moves as part of the rigid Australian Plate, as it has been suggested or assumed by several studies [e.g. *Tregoning, 2002, 2003; Wallace et al., 2004; Sella et al., 2007; Argus, 2010; Altamimi et al., 2012*] that Auckland (AUCK, see Figure 6) lies on the Australian Plate. Note that motion of sites in the central and eastern regions of the North Island regularly experience non-linear motion as a result of slow slip events on the Hikurangi Trench [e.g. *Wallace et al., 2004; Wallace and Beavan, 2006*] and we do not attempt to estimate residual linear velocities in this region.

Our analysis of a network of sites along the west coast of the North Island of New Zealand shows significant motion relative to our model of the rigid Australian Plate (Figure 6). The pattern of relative velocities can be modelled as a rigid block rotation of  $\sim 0.28 \pm 0.03^\circ/\text{My}$  about an Euler pole located at  $S35.78^\circ, E171.25^\circ$ . This would be consistent with possible transform motion on the van der Linden Fault and the Vening Meinesz Fracture Zone north of the North Island [*Sutherland, 1999*]. Alternatively, the deformation could indicate inter-seismic strain accumulation associated with the Australia-Pacific Plate boundary that will be released by the next great earthquake or slow slip event in the region. In either case, none of the sites spanning the North Island of New Zealand should be considered to be moving as part of the rigid Australian Plate.

#### 4.2. Tectonic interpretation from an alternate coordinate reference frame definition

To demonstrate how the definition of the terrestrial reference frame influences the horizontal velocities derived from the time series of GPS coordinates, we generated a second set of site velocities from our daily GPS solutions, this time using a different set of sites and discontinuities to define the reference frame. For this second solution, we used  $\sim 30$ -40 of the core IGS sites [*Reibischung et al., 2012*] and the associated set of offsets that comprise the IGS2008. This includes several sites on the Australian Plate and some of the sites for which our solutions show non-linear motion (e.g. HOB2, TIDB). The time series generated in this manner typically have a higher level of noise, which we attribute to the hydrological loading and possible discontinuities/non-linear motions at the additional core sites propagating through the transformation into the coordinates of other sites.

We generated an estimate of the Euler vector for the Australian Plate using the same set of sites to define the plate motion as was used in ITRF2008 [*Altamimi et al., 2012*], then computed residual velocity vectors with respect to this definition of the plate motion (blue vectors in Figure 5). Of the 14 sites on the Australian continent, only three of the error ellipses (95% confidence level) of the residual horizontal velocities overlap between our preferred solution and that of the second solution (using the ITRF2008 core sites to stabilise the reference frame plus the enlarged selection of sites to define the Australian Plate motion). In some cases, the

residuals are considerably larger than those of our preferred solution. For example, convergence of  $\sim 0.7 \pm 0.14$  mm/yr ( $1\sigma$ ) is implied between Ceduna and Adelaide, whereas our preferred solution shows  $-0.2 \pm 0.2$  mm/yr ( $1\sigma$  uncertainties). Additionally, the relative residual vectors at Burnie and Hobart, Tasmania, suggest extension of  $\sim 2.2 \pm 0.3$  mm/yr across Tasmania and convergence of  $\sim 2.2 \pm 0.3$  mm/yr between Tasmania and Adelaide. There is no tectonic evidence for any of these motions. Furthermore, all of these sites have been used to define the rigid motion of the Australian Plate so, by construction, one would not expect to find relative motion between the sites.

Not accounting for non-linear deformation signals caused by distant great earthquakes degrades the accuracy of linear velocity estimates. Our horizontal velocity estimate for Hobart using only data prior to the 2004 Macquarie Ridge earthquake is  $56.15 \pm 0.07$  and  $14.03 \pm 0.06$  mm/yr for the north and east components, respectively (north component is shown in Figure 3), compared to  $55.67 \pm 0.12$  and  $14.34 \pm 0.08$  mm/yr when fitting a linear trend through all the observations, including the post-seismic period (we applied the ITRF2008 offset to correct for the co-seismic displacement at HOB2 but make no correction for the post-seismic relaxation since this is not accounted for in ITRF2008). Velocity errors of  $\sim 0.3$  mm/yr and  $\sim 0.05$  mm/yr also occur at MOBS and TIDB, respectively, showing a decrease in error further away from the earthquake epicentre. Thus, failing to account for far-field post-seismic deformation can introduce velocity errors as large as 0.5 mm/yr, larger than the uncertainties of the velocity estimates and significantly larger than the level of rigidity of the western part of the Australian Plate.

Additionally, we estimated residual velocity vectors for the sites in the North Island of New Zealand with respect to this second definition of the motion of the Australian Plate (blue arrows in Figure 6). The rotation of the western North Island w.r.t. the Australian Plate that is seen in the residual velocities of our preferred solution is no longer evident, with the sites north of  $\sim S37^\circ$  showing insignificant motion relative to the Australian Plate - probably caused by the inclusion of the velocities of two sites in Auckland into the definition of the Australian Plate motion. In this

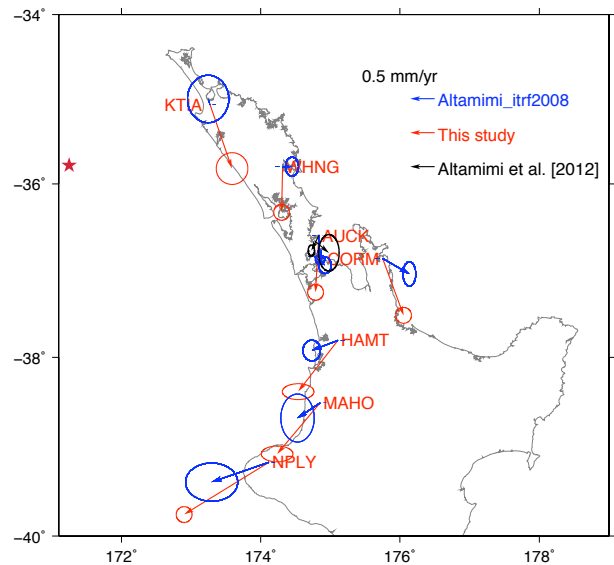


**Figure 5.** As for Figure 5, but showing the residual velocities for sites in the North Island of New Zealand. The relative pole of rotation that fits these vectors is indicated with a star.



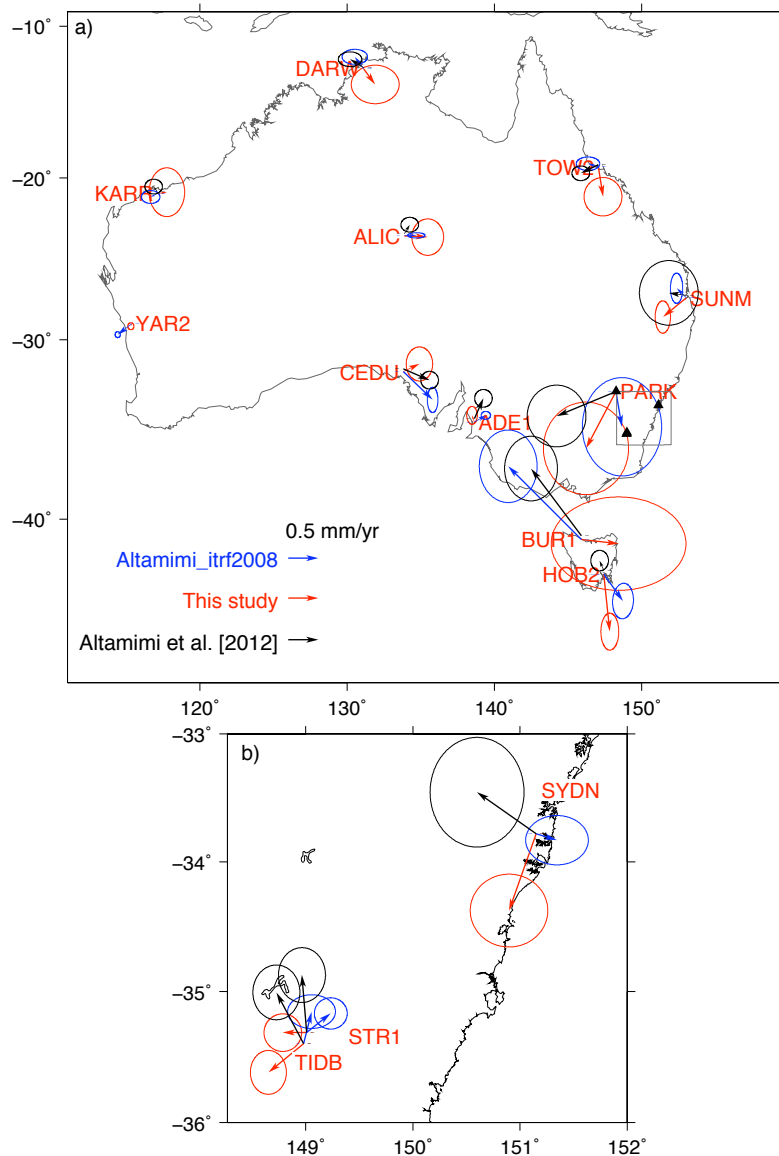


**Figure 6.** a) Horizontal velocity residuals of GPS sites on the Australian Plate using our definition of the reference frame plus only 6 sites (YAR2, KARR, DARW, ALIC, CEDU, ADE1) to define the Australian Plate motion (red), and using the core IGS sites to define the reference frame plus the sites of *Altamimi et al.* [2012] to define the Australian Plate motion (blue). ITRF2008 residual velocities of *Altamimi et al.* [2012] are shown in black. b) Zoom showing the velocity residuals at the sites in Canberra and Sydney.

latter solution, right-lateral strike slip motion is required between Auckland and Hamilton, whereas in our preferred the residual velocities can be explained by a block rotation of the entire region relative to the Australian Plate. Thus, the more general selection of key sites from which to define the terrestrial reference frame and the rigid Australian Plate leads to less clarity in the interpretation of the residual velocities, and requires small crustal deformations between certain sites when there is no evidence for such tectonic activity.

## 5. Conclusions

Earthquakes account for much of the deformation of the Earth's surface and large earthquakes will continue to cause measurable step offsets in geodetic position time series. Between 1 and 20 earthquakes of  $M_w > 8$  occur each decade, deforming around 50% of the surface of the Earth with am-

plitudes  $> 1$  mm. Areas along particular nodal lines of the great earthquakes, at the extensions of the strikes of the fault ruptures, experience the smallest amounts of deformation. Thus, defining and maintaining a stable terrestrial reference frame over multiple decades to support studies of the dynamic Earth system is extremely problematic because, at unknown and irregular intervals, virtually the entire tracking network will move abruptly in an unpredictable manner. We have shown that this deformation can induce linear velocity errors of up to 0.4 mm/yr at sites over 1000 km from the earthquake locations.

However, it is possible to mitigate the consequences of these problems and thus generate secular motion estimates with accuracies of 0.2 mm/yr or better through the careful selection of reference sites in nodal areas of least co-seismic deformation. Thus, through an adaptive process, earthquake deformations at other sites could then be corrected, resulting in a long-term, stable reference frame. With a careful selection of sites to define the terrestrial reference frame,

sub-mm accuracy of site velocities is possible over decadal time scales at the level claimed for the most recent International Terrestrial Reference Frame [Altamimi *et al.*, 2012], but it is important that changes in instrument hardware that cause coordinate offsets are first detected and removed with the highest accuracy possible.

Despite the occurrence of a high number of great earthquakes, including three on its plate boundaries, a large portion of the Australian Plate (excluding the SE regions of Tasmania, Victoria and parts of New South Wales) is deforming at  $< 0.2$  mm/yr, making it one of the most stable crustal regions in the world. However, motion of GPS sites located even thousands of kilometres from active interplate boundaries can still be contaminated by earthquake deformations. The improved resolution of our GPS analysis permitted the identification of non-linear post-seismic relaxation along the east coast of Australia, as noted previously by Watson *et al.* [2010]. We note that this post-seismic deformation is not considered in ITRF2008 [Altamimi *et al.*, 2011, 2012] but amounts to  $\sim 5$ -10 mm in the 5 years following the Macquarie Ridge earthquake.

While small in magnitude, both earthquake and instrument effects must first be accounted for in order to be able to identify the true level of intra-plate rigidity and to recognise local deviations from it. Careful selection of sites located on the 'rigid' part of tectonic plates is also important; otherwise, incorrect interpretations of the residual deformation fields can occur as demonstrated for the case of southeast Australia and the North Island of New Zealand. The detection of small-magnitude crustal deformations can only be drawn from state-of-the-art GPS analysis and modelling, accounting first for time varying atmospheric effects, atmospheric pressure loading deformation, co-seismic earthquake deformation of distant earthquakes and instrument offset identification.

**Acknowledgments.** This research was supported under the Australian Research Council's Discovery Projects funding scheme (DP0877381). We thank the IGS for making global GPS data freely available and Frank Pollitz for sharing his spherical earthquake deformation code. Figures were plotted using GMT [Wessel and Smith, 1998]. Part of this work was conducted while SL was on sabbatical at ANU. The GPS data were computed on the Terrawulf II computational facility at the Research School of Earth Sciences, a facility supported through the AuScope initiative. AuScope Ltd is funded under the National Collaborative Research Infrastructure Strategy (NCRIS), an Australian Commonwealth Government Programme. We thank the Associate Editor and two anonymous reviewers for review comments.

## References

- Altamimi, Z., X. Collilieux, and L. Métivier (2011) ITRF2008: an improved solution of the International Terrestrial Reference Frame, *J. Geod.*, 85, 457-473, doi:10.1007/s00190-011-0444-4
- Altamimi, Z., L. Métivier and X. Collilieux (2012) ITRF2008 Plate Motion Model *J. Geophys. Res.*, 117, B07402, doi:10.1029/2011JB008930.
- Banerjee, P., et al (2007) Coseismic slip distributions of the 26 December 2004 Sumatra-Andaman and 28 March 2005 Nias earthquakes from GPS static offsets, *Bull. Seis. Soc. Am.*, 97, S86-S102.
- Beavan, J., et al. (2010) Near-simultaneous great earthquakes at Tongan megathrust and outer rise in September 2009, *Nature*, 466(7309), 959-U978.
- Beckley, B. D., F. G. Lemoine, S. B. Luthcke, R. D. Ray, and N. P. Zelensky (2007) A reassessment of global and regional mean sea level trends from TOPEX and Jason-1 altimetry based on revised reference frame and orbits, *Geophys. Res. Lett.*, 34, L14608, doi:10.1029/2007GL030002.
- Chao, B. F. and R. S. Gross (1987) Changes in the Earth's rotation and low-degree gravitational field induced by earthquakes, *Geophys. J. Royal Astr. Soc.*, 91, 569-596.
- Dziewonski, A.M. and D.L. Anderson (1981) Preliminary reference Earth model, *Phys. Earth Planet. Int.*, 25, 297-356.
- Ekström, G., M. Nettles and A.M. Dziewoński (2012) The global CMT project 2004-2010: Centroid-moment tensors for 13,017 earthquakes, *Phys. Earth Planet. Int.*, 200201, 1-9, 10.1016/j.pepi.2012.04.002.
- Featherstone, W.E., M.S. Filmer, N.T. Penna, L.M. Morgan and A. Schenk (2012) Anthropogenic land subsidence in the Perth Basin: challenges for its retrospective geodetic detection, *J. Royal Soc. Western Aust.*, 95, 5362.
- Fu, G. and W. Sun (2006) Global co-seismic displacements caused by the 2004 Sumatra-Andaman earthquake (Mw 9.1), *Earth, Planets, Space*, 58, 149-152.
- Furlong, K.P., T. Lay and C.J. Ammon (2009) A Great Earthquake Rupture Across a Rapidly Evolving Three-Plate Boundary, *Science*, 324, 226-229.
- Gordon, R.G. (1998) The plate tectonic approximation: plate nonrigidity, diffuse plate boundaries, and global plate reconstructions, *Annu. Rev. Earth Planet. Sci.*, 26, 615-642.
- Gross, R. S. and Chao, B. F. (2006) The rotational and gravitational signature of the December 26, 2004 Sumatran earthquake, *Surv. Geophys.*, 27, 615-632.
- Konca, A. O., et al. (2008) Partial rupture of a locked patch of the Sumatra megathrust during the 2007 earthquake sequence, *Nature*, 456(7222), 631-635.
- Kreemer, C., Blewitt, G., Hammond, W.C. and H-P Plag (2006) Global deformation from the great 2004 Sumatra-Andaman Earthquake observed by GPS: Implications for rupture process and global reference frame, *Earth, Planets, Space*, 58, 141-148.
- Lay, T., H. Kanamori, C. J. Ammon, A. R. Hutko, K. Furlong, and L. Rivera (2009) The 2006/2007 Kuril Islands great earthquake sequence, *J. Geophys. Res.*, 114, B11308, doi:10.1029/2008JB006280.
- Lay, T., et al. (2010) The 2009 Samoa-Tonga great earthquake triggered doublet, *Nature*, 466(7309), 964-U985.
- Lorito, S., et al. (2011) Limited overlap between the seismic gap and coseismic slip of the great 2010 Chile earthquake, *Nat. Geosci.*, 4(3), 173-177.
- Park, S.-C., and J. Mori (2007) Triggering of earthquakes during the 2000 Papua New Guinea earthquake sequence, *J. Geophys. Res.*, 112, B03302, doi:10.1029/2006JB004480.
- Pollitz, F.F. (1996) Coseismic deformation from earthquake faulting on a layered spherical earth, *Geophys. J. Int.*, 125, 1-14.
- Pritchard, M. E., E. O. Norabuena, C. Ji, R. Boroschek, D. Comte, M. Simons, T. H. Dixon, and P. A. Rosen (2007) Geodetic, teleseismic, and strong motion constraints on slip from recent southern Peru subduction zone earthquakes, *J. Geophys. Res.*, 112, B03307, doi:10.1029/2006JB004294.
- Reilinger, R., et al. (2006) GPS constraints on continental deformation in the Africa-Arabia-Eurasia continental collision zone and implications for the dynamics of plate interactions, *J. Geophys. Res.*, 111, B05411, doi:10.1029/2005JB004051.
- Rothacher, M. et al. (2009) The future Global Geodetic Observing System, in *Global Geodetic Observing System: Meeting the Requirements of a Global Society on a Changing Planet in 2020*, Plag, H.-P. and Pearlman, M. (Eds.), Springer, 237-270.
- Romano, F., A. Piatanesi, S. Lorito, and K. Hirata (2010) Slip distribution of the 2003 Tokachi-oki Mw 8.1 earthquake from joint inversion of tsunami waveforms and geodetic data, *J. Geophys. Res.*, 115, B11313, doi:10.1029/2009JB006665
- Simons, M., et al. (2011) The 2011 magnitude 9.0 Tohoku-Oki earthquake: Mosaicking the megathrust from seconds to centuries, *Science*, 332(6036), 1421-1425.
- Sladen, A., H. Tavera, M. Simons, J. P. Avouac, A. O. Konca, H. Perfettini, L. Audin, E. J. Fielding, F. Ortega, and R. Cavagnoud (2010), Source model of the 2007 Mw 8.0 Pisco, Peru earthquake: Implications for seismogenic behavior of subduction megathrusts, *J. Geophys. Res.*, 115, B02405, doi:10.1029/2009JB006429.
- Steigenberger, P. J. Boehm and P. Tesmer (2009) Comparison of GMF/GPT with VMF1/ECMWF and implications for atmospheric loading, *J. Geod.*, 83, 943-951.
- Sutherland, R. (1999) Basement geology and tectonic development of the greater New Zealand region: an interpretation from regional magnetic data, *Tectonophysics*, 308, 341-362.
- Tang, L., V. V. Titov, Y. Wei, H. O. Mofjeld, M. Spillane, D. Arcas, E. N. Bernard, C. Chamberlin, E. Gica, and J. Newman (2008), Tsunami forecast analysis for the May 2006 Tonga tsunami, *J. Geophys. Res.*, 113, C12015, doi:10.1029/2008JC004922.

- Tregoning, P. and C. Watson (2009) Atmospheric effects and spurious signals in GPS analyses, *J. Geophys. Res.*, 114, B09403, doi:10.1029/2009JB006344
- Tregoning, P., C. Watson, G. Ramillien, H. McQueen and J. Zhang (2009) Detecting hydrologic deformation using GRACE and GPS, *Geophys. Res. Lett.*, 36, L15401, doi:10.1029/2009GL038718.
- Vigny, C., et al., (2005) Insight into the 2004 Sumatra-Andaman earthquake from GPS measurements in Southeast Asia, *Nature*, 436, 201206.
- Wallace, L. M., J. Beavan, R. McCaffrey, and D. Darby (2004), Subduction zone coupling and tectonic block rotations in the North Island, New Zealand, *J. Geophys. Res.*, 109, B12406, doi:10.1029/2004JB003241.
- Wallace, L.M. and J. Beavan (2006) A large slow slip event on the central Hikurangi subduction interface beneath the Manawatu region, North Island, New Zealand *Geophys. Res. Lett.*, 33, L11301, doi:10.1029/2006GL026009.
- Watson, C.S., R. Burgette, P. Tregoning, N. White, J. Hunter, R. Coleman, R. Handsworth and H. Brolsma (2010) Twentieth Century constraints on sea level change and earthquake deformation at Macquarie Island, *Geophys. J. Int.*, doi:10.1111/j.1365-246X.2010.04640.x
- Wessel, P., and W. H. F. Smith (1998) New, Improved Version of Generic Mapping Tools Released, *EOS Trans.*, AGU, 79 (47), p. 579.
- Williams., S, and N. Penna (2011) Non-tidal ocean loading effects on geodetic GPS heights, *Geophys. Res. Lett.*, 38, L09314., doi:10.1029/2011GL046940
- Yagi, Y. and Y. Fukahata (2011) Rupture process of the 2011 Tohoku-oki earthquake and absolute elastic strain release, *Geophys. Res. Lett.*, 38, L19307, doi:10.1029/2011GL048701.
- 
- S. Lejeune, Royal Meteorological Institute of Belgium, Brussels, Belgium
- S. C. McClusky, H. McQueen, P. Tregoning, Research School of Earth Sciences, The Australian National University, Canberra, ACT, Australia. (Paul.Tregoning@anu.edu.au)
- R. Burgette, C.S. Watson, Surveying and Spatial Science Group, School of Geography and Environmental Studies, University of Tasmania, Hobart, TAS, Australia